Hierarchical assembly of native cytoplasmic lattices revealed by cryo-EM

Yin-Li Zhang[1#], Yuqi Liu[1,2#], Qi Liu[1,2#], Qi Zhang[1#], Jiamin Jin[1], Siya Liu[1], Shuo Yang[2], Yinan Liu[2], Ye-Jun Peng[2], Mengru Lai[1], Yuting Sun[1], Ying-Yi Zhang[1], Yuqing Mei[1], Xiaomei Tong[*1], Songying Zhang[*1], Miao Gui[*1,2]

https://doi.org/10.15302/vita.2026.04.0030

Dear Editor,

Mammalian oocytes accumulate extensive reservoirs of maternal proteins that sustain fertilization and early embryonic development[1]. Central to this regulatory framework are cytoplasmic lattices (CPLs), specialized filamentous assemblies present in mammalian oocytes and preimplantation embryos that organize and stabilize intracellular constituents[1,2]. Genetic approaches have identified several maternal-effect genes in humans — including *PADI6*, *NLRP5*, *TLE6* and *OOEP* — as essential for CPL formation, since their mutation disrupts CPL integrity and leads to early embryonic arrest and female infertility[1]. Early studies have characterized the general morphology of CPLs[3] and the structures of recombinant subcomplexes such as the subcortical maternal complex (SCMC)[4], yet the exact molecular composition and assembly mechanism remain elusive. Here, we use cryo-electron microscopy (cryo-EM) to resolve the near-atomic structure of native CPLs from mouse oocytes, identifying at least fourteen proteins organized into periodic filaments that further assemble into helical bundles. These findings demonstrate that CPLs function as a multifunctional hub for the storage and coordinated regulation of cytoskeletal elements and protein degradation machinery. Complemented by proteomics and *in vitro* recombinant studies, we propose a model for the hierarchical assembly of CPLs, from subcomplexes to filaments to supramolecular lattices.

To determine the high-resolution structure of endogenous CPLs, we developed a cell-lysis-on-grid (CLoG) approach, in which 400–500 oocytes of the germinal vesicle (GV) stage were lysed on cryo-EM grids prior to data collection (Fig. 1a). An integrated particle-picking strategy was employed to select CPL filaments, yielding a consensus reconstruction of the repeating unit with overall C2 symmetry and local asymmetry features (Supplementary Fig. S1 and Table S1). Local refinements improved the maps to a resolution of up to 3.4 Å, permitting unambiguous assignment of fourteen proteins and building of their atomic models (Supplementary Fig. S2 and Tables S2, S3). The CPL filament features periodic bulbous swellings separated by narrower segments, with an axial repeat of approximately 37 nm (Fig. 1b), which is consistent with the structural features of the CPLs within mouse oocytes, as determined by *in situ* cryo–electron tomography (cryo–ET)[3].

In CPLs, polymers of PADI6 and SCMCs (comprising NLRP5, TLE6, OOEP, KHDC3 or ZBED3) form the primary scaffold at the periphery of each bulbous unit (Fig. 1b). Functional modules UHRF1–UBE2D3, SKP1–FBXW, and α/β-tubulin localize to the central core region. Two NLRP family members — NLRP4f and NLRP14 — bridge longitudinal continuity and lateral interactions of CPLs, respectively. Together, these components assemble into a densely interconnected molecular network that reinforces the structural integrity of the CPLs. The structural organization and protein assignments were validated by cross-linking mass spectrometry (XL-MS) (Fig. 1c; Supplementary Fig. S3 and Tables S4, S5). In addition, reanalysis of published proteomic, Ribo-seq and RNA-seq datasets from mouse oocytes and early embryos spanning developmental stages confirmed high expression of CPL components from GV oocytes to 8-cell embryos[5,6] (Supplementary Fig. S4). To further validate protein interactions, we performed co-immunoprecipitation (co-IP) coupled with MS using mouse GV oocytes microinjected with cRNAs encoding Flag-tagged PADI6 or OOEP (Supplementary Fig. S5). UHRF1 and UBE2D3 were specifically enriched in the PADI6 interactome, whereas all five SCMC components were enriched in the OOEP group. These results support the existence of tightly associated subcomplexes — such as PADI6–UHRF1–UBE2D3 and SCMC[4,7] — that likely function as modular building blocks for the assembly of CPL filaments.

PADI6 is a well-characterized maternal factor whose mutations cause early embryonic arrest and female infertility in both humans and mice[8]. Within CPLs, at least five PADI6 dimers assemble into a hollow tubular structure at each lateral edge of the bulbous unit (Fig. 1d). The PADI6 tubule adopts an imperfect helical architecture, with a variable helical rise ranging from 2.6 to 4.1 nm and a helical twist of 90° to 128° (Supplementary Fig. S6a). This assembly is primarily mediated by interactions between the N-terminal (PAD-N) and middle (PAD-M) IgG domains of adjacent dimers (Supplementary Fig. S6d, e).

To investigate whether PADI6 can self-assemble into higher-order structures analogous to those observed in CPLs, we expressed and purified mouse PADI6 and analyzed its oligomeric state by sucrose gradient ultracentrifugation with cross-linker BS3. In addition to the expected monomeric and dimeric species, SDS-PAGE revealed prominent high-molecular-weight bands, indicating the formation of higher-order assemblies (Supplementary Fig. S6g). Cryo-EM revealed a heterogeneous population comprising one to eight dimers (Supplementary Figs. S6f, S7). Notably, the inter-dimer assembly packing closely resembles that observed in CPLs, both exhibiting a more compact arrangement in the center rela-

1. Assisted Reproduction Unit, Department of Obstetrics and Gynecology, Sir Run Run Shaw Hospital, Zhejiang Key Laboratory of Precise Protection and Promotion of Fertility, Zhejiang Provincial Clinical Research Center for Reproductive Health and Disease, Zhejiang University School of Medicine, Hangzhou, Zhejiang, China. 2. Liangzhu Laboratory, Zhejiang University School of Medicine, Hangzhou, Zhejiang, China. #These authors contributed equally. *Correspondence: Xiaomei Tong (3406028@zju.edu.cn), Songying Zhang (zhangsongying@zju.edu.cn), Miao Gui (miaogui@zju.edu.cn)

Received: March 30, 2026; Accepted: April 27, 2026; Published: May 8, 2026

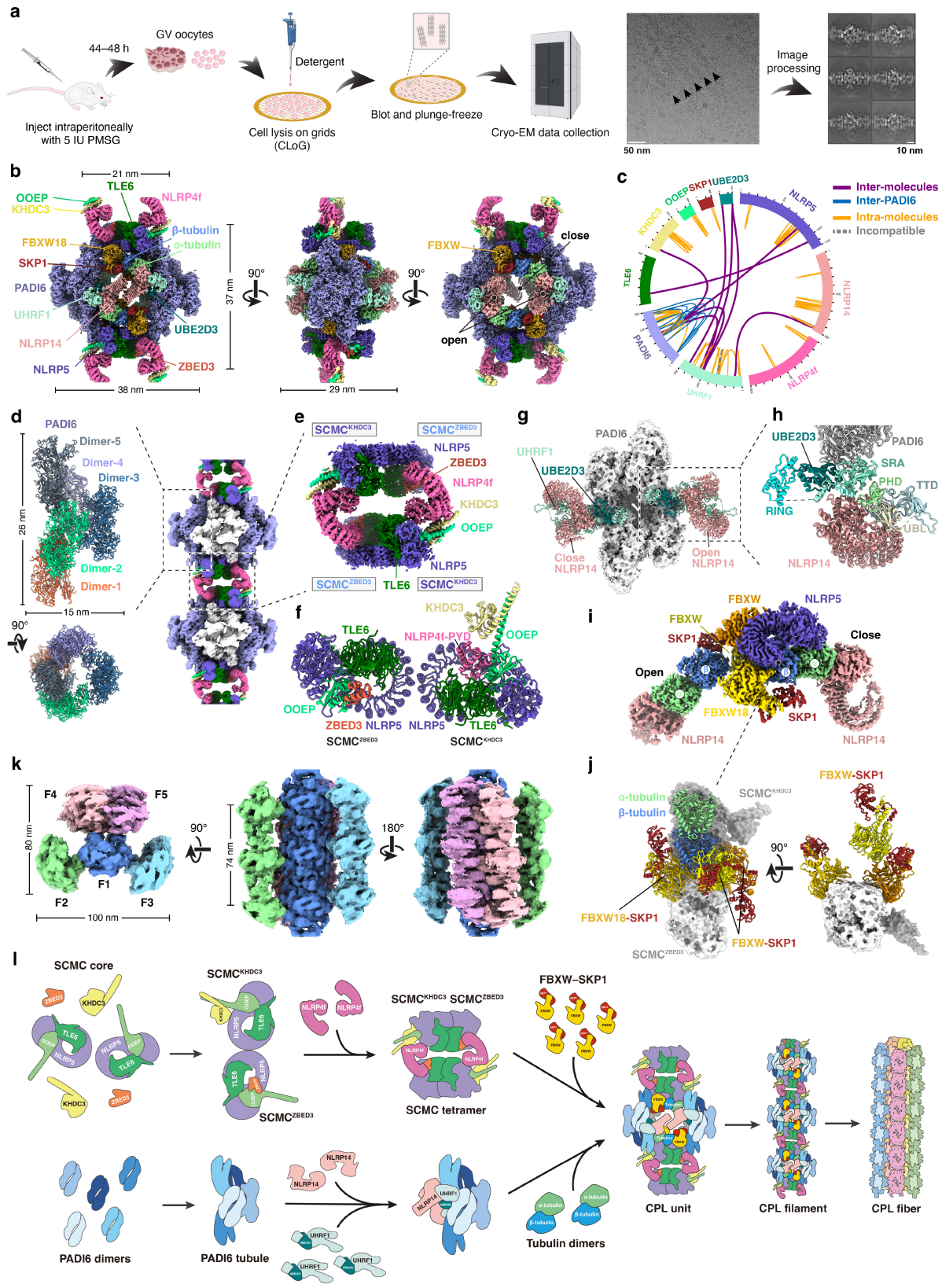

Fig. 1 Structure and assembly mechanism of native mouse CPLs. a Workflow diagram for cryo-EM of native mouse CPLs. **b** Cryo-EM map of one repeating unit of the CPLs. **c** XL-MS analysis of mouse CPLs, highlighting cross-links among CPL components. **d** Model of PADI6 assembly in CPLs. Each PADI6 dimer is shown with a distinct color. **e** Model of SCMC complexes in CPLs. **f** Dimerization of SCMC^{KHDC3} and SCMC^{ZBED3} mediated by the LRRs of NLRP5. **g** Model of PADI6 tubule and its associated UHRF1–UBE2D3–NLRP14 modules. PADI6 is shown in surface presentation. **h** Zoom-in view showing the domain organization of UHRF1 and the interaction with UBE2D3, PADI6 and NLRP14. **i** Cryo-EM map of two α/β-tubulin heterodimers and their associated proteins. **j** Three SKP1–FBXW dimers associate with an SCMC dimer and an α/β-tubulin heterodimer. **k** Cryo-EM map of the five-helical bundle structure of CPLs. **l** Cartoon diagram showing the hierarchical assembly of CPLs.

tive to the terminal dimers (Supplementary Fig. S6a–c). Interactions at the inter-dimer interface — including contacts between R43 and Y123, and between W66 and N145 — mediate tubular assembly, and disruption of these interactions

impairs the higher-order oligomerization of PADI6 (Supplementary Fig. S6g, h). Collectively, these findings establish that PADI6 dimers function primarily as a structural scaffold through their intrinsic polymerization capacity, providing the foundational framework for CPL assembly.

Unexpectedly, our structure revealed two distinct subtypes of SCMCs, one comprising NLRP5, TLE6, OOEP and KHDC3 ($SCMC^{KHDC3}$) and another in which KHDC3 is replaced by ZBED3 ($SCMC^{ZBED3}$) (Fig. 1e; Supplementary Fig. S8). Dimerization of $SCMC^{KHDC3}$ and $SCMC^{ZBED3}$ is mediated by the leucine-rich repeats (LRRs) of NLRP5 molecules (Fig. 1f), consistent with the recombinant SCMC structures[4]. In $SCMC^{KHDC3}$, the K Homology (KH) domain of OOEP interacts with the N-terminal pyrin domain (PYD) of NLRP4f, while the C-terminal helix of OOEP engages KHDC3 (Fig. 1f). In $SCMC^{ZBED3}$, ZBED3 replaces the NLRP4f PYD to interact with the SCMC core, which further interacts with the C-terminal LRR of NLRP4f (Supplementary Fig. S8d). Thus, two SCMC dimers are bridged by two NLRP4f molecules to form a hollow, centrosymmetric assembly that links adjacent bulbous units and promotes CPL filament formation.

To dissect the functional contribution of SCMC components to CPL assembly and embryogenesis, we generated *Ooep*$^{-/-}$ mice (Supplementary Fig. S9). Female *Ooep*$^{-/-}$ mice were infertile, and the majority of embryos arrested at the two-cell to four-cell stages (Supplementary Fig. S9b–d), consistent with previous reports[9]. Of note, all SCMC components were markedly reduced in abundance in *Ooep*$^{-/-}$ oocytes (Supplementary Fig. S9e–l), mirroring observations in *Tle6* knockout mice[3]. This interdependence aligns with our structural finding that SCMC constituents assemble into a stable complex, wherein depletion of core members destabilizes the entire assembly. Ultrastructural analysis further demonstrated a complete absence of CPL filaments in *Ooep*$^{-/-}$ oocytes (Supplementary Fig. S9m). Indeed, depletion of any individual SCMC component has been reported to disrupt CPL formation (Supplementary Table S6), indicating that these proteins are collectively essential for CPL formation.

Within each asymmetric unit of the CPL bulbous repeat, two UHRF1–UBE2D3 heterodimers occupy equivalent binding sites on the PADI6 tubule, and each recruits one NLRP14 molecule (Fig. 1g, h). This quasi-centrosymmetric geometry orients the UHRF1–UBE2D3 modules and their associated NLRP14 partners in opposing directions, placing one NLRP14 in a "closed" conformation and the other in an "open" configuration (Fig. 1g; Supplementary Fig. S10a). Consistent with their direct physical interaction, loss of NLRP14 reduces UHRF1 protein abundance, and *vice versa*[10,11]. CPLs also harbor a second ubiquitination-related module, heterodimers of SKP1–FBXW (Fig. 1i). Five SKP1–FBXW heterodimers were identified in each repeating unit of CPLs, and two were assigned as FBXW18 based on the sidechain density (Supplementary Fig. S10d, e). These SKP1–FBXW modules are deeply embedded within the CPL architecture, making them inaccessible to both the Cullin-RING catalytic machinery and potential substrates (Supplementary Fig. S10f). Furthermore, UHRF1 is also maintained in an inactive conformation when incorporated into CPLs, with its key interaction surfaces for DNA, histones and Stella sequestered by intra-complex contacts (Supplementary Fig. S10b, c). This spatial sequestration suggests a structural mechanism in which the temporal control of ubiquitin-mediated proteostasis regulates early development. Consistently, siRNA knockdown of *Skp1* or *Ube2d3* resulted in a pronounced loss of CPL filaments (Supplementary Fig. S11).

How do CPLs interact with the conventional cytoskeleton? We identified four α/β-tubulin dimers embedded within the CPL bulbous repeat (Supplementary Fig. S12). Within each asymmetric unit, one tubulin dimer associates with the open NLRP14, whereas the other engages the closed conformation, thereby positioning one α/β-tubulin dimer closer to the core of the bulbous unit and the SCMC, and the other at a more peripheral location (Fig. 1i, j). Despite these distinct spatial arrangements, the α-tubulin–NLRP14 interface is conserved between the two states, while the β-tubulin exhibits differential interactions with SKP1–FBXW (Supplementary Fig. S12c–h). The high-resolution cryo-EM map reveals that both α- and β-tubulins are bound to GTP and Mg^{2+} (Supplementary Fig. S12i). Structural superposition further shows that tubulins within CPLs closely resemble the conformation of GMPCPP-bound tubulin dimers, but differ markedly from the tubulins observed in assembled microtubules (MTs) (Supplementary Fig. S12j–m). The retention of a GTP-bound, assembly-competent conformation suggests that CPLs harbor a reservoir of polymerization-ready tubulins, poised to support rapid MT assembly upon release.

Importantly, we also resolved four pairs of double-filament CPLs which could be further assembled into a complete five-helical bundle structure (Fig. 1k), consistent with the cryo-ET observation[3]. Within this assembly, four peripheral filaments associate with a central filament through conserved NLRP14–PADI6 interactions (Supplementary Fig. S13). In addition, UHRF1 likely contributes to inter-filament coupling by engaging an unassigned density of neighboring filaments. Further multivalent interactions involving PADI6, open-state NLRP14 and SCMC components from the F4 and F5 filaments reinforce lateral association (Supplementary Fig. S13g, h). Together, these findings establish that open-state NLRP14, UHRF1 and PADI6 serve as principal mediators of inter-filament connectivity.

In this work, we developed an efficient CLoG strategy and determined the cryo-EM structure of native CPLs. We identified both well-characterized and understudied factors and elucidated their detailed molecular interactions. These findings provide a mechanistic foundation for understanding how oocyte proteins govern CPL assembly. Three recent structural studies of CPLs from GV oocytes were published when we were preparing our manuscript[12–14]. While those studies characterized the core CPL architecture, our work provides critical additional insights, including the principles governing higher-order CPL assembly, the structural basis of recombinant PADI6 polymers that scaffold CPLs, and the functional roles of OOEP, SKP1 and UBE2D3 in regulating CPL formation and early embryogenesis using mouse and cell models. In addition, two recent preprints have resolved CPL structures at later developmental stages (MII oocytes and six- to eight-cell embryos)[15,16], revealing that the E2 ligase within embryonic CPLs is competent for ubiquitin charging while the overall architecture is preserved.

The reconstituted SCMC core forms a stable complex that can dimerize[4]. Our structure further reveals that the incorporation of accessory SCMC proteins (KHDC3 and ZBED3) and NLRP4f organizes four SCMCs into a hollow tetrameric assembly. Depletion of any of these five SCMC proteins or NLRP4f disrupts CPL formation in mice (Supplementary Table S6). Notably, loss of KHDC3, ZBED3 or NLRP4f does not markedly

affect expression of the SCMC core proteins, whereas depletion of *Ooep* or *Tle6* drastically reduces the levels of all SCMC components (Supplementary Fig. S9j, k). Consistently, knockout of *Khdc3*, *Zbed3*, or *Nlrp4f* results in delayed preimplantation development and reduced fecundity — phenotypes less severe than the early embryonic arrest and female sterility observed in *Nlrp5*, *Tle6*, or *Ooep* knockout mice (Supplementary Table S6). This asymmetric dependency indicates that while accessory proteins are required for proper CPL assembly, the SCMC core subcomplex remains intact in their absence and can partially support oocyte function.

Another unexpected finding is that PADI6 dimers self-assemble into hollow tubules both in native CPLs and *in vitro*. These PADI6 tubules interconnect with super-SCMC tetramers throughout the CPL, together forming its principal structural scaffold. Interestingly, most SCMC components were not particularly enriched by Flag-PADI6 pull-down (Supplementary Fig. S5b), and their protein levels remained largely unchanged upon *Padi6* knockout (Supplementary Fig. S12n). These observations suggest that PADI6 and the SCMC initially assemble into distinct subcomplexes that are subsequently integrated into CPL filaments through relatively weak interactions. In contrast, the abundance of the UHRF1–UBE2D3–NLRP14 module is strongly dependent on PADI6 and this dependency is unidirectional, as depletion of UHRF1 does not affect PADI6 levels (Supplementary Fig. S12n–p).

Taken together, the structural organization of CPLs and the identification of subcomplexes, together with the unidirectional dependencies between the SCMC core and accessory factors, and between PADI6 and its partners, support a hierarchical assembly pathway for CPLs (Fig. 1l). Lateral interactions involving NLRP14, UHRF1 and PADI6 further promote inter-filament associations, giving rise to the characteristic five-helical-bundle configuration, which may recruit additional CPL filaments to form the lattice architecture. However, the mechanism underlying CPL disassembly awaits future investigation (Supplementary Fig. S14). Many of the CPL components are maternal-effect genes and their gene variants have frequently been linked to early embryonic arrest, multilocus imprinting disorders or hydatidiform molar pregnancies (Supplementary Table S6). The variants are distributed throughout the structure within PADI6, NLRP14, UHRF1 and four SCMC components, with a concentration in SCMC and PADI6 (Supplementary Fig. S15 and Table S7). Moreover, our work revealed the exact composition of mouse CPLs, which provides a confident list of candidate pathogenetic genes for future molecular diagnosis of female infertility. Taken together, our study offers mechanistic insights into how maternal proteins are spatially organized to ensure successful early embryonic development and lays the foundation for targeted therapeutic strategies aimed at addressing fertility disorders and genomic imprinting defects related to CPL-associated gene mutations.

DATA AVAILABILITY

Cryo-EM maps have been deposited in the Electron Microscopy Data Bank under accession numbers EMD-69647, EMD-69606, EMD-69605, EMD-69604, EMD-69603, EMD-69601, EMD-69599, EMD-69566, EMD-69583, EMD-69573, EMD-69578, EMD-69579, EMD-69582, EMD-69581, EMD-69608, EMD-69633, EMD-69635, EMD-69637, EMD-69638 and EMD-69639. The atomic model of CPLs has been deposited in the Protein Data Bank under accession number 24MC.

ACKNOWLEDGEMENTS

We thank the Cryo-EM Facilities of Liangzhu Laboratory and Shuimu BioSciences for data collection and computation, and the Core Facility of Liangzhu Laboratory for technical assistance. We thank Xiaolin Tian and Haiteng Deng in the Center of Protein Analysis Technology, Tsinghua University, for XL-MS analysis. This work was supported by the National Key R&D Program of China (2025YFA1309900 to M.G., 2022YFC 2702300 to Y.Z.), the National Natural Science Foundation of China (32471245 to M.G., U23A20403 to S.Z.), the Zhejiang Provincial Natural Science Foundation of China (LZ24C050001 and LR26C050002 to M.G., LD26H040001 to Y.Z.), and the Zhejiang Provincial Leading Innovation and Entrepreneurship Team Introduction and Cultivation Program (2024R01024 to M.G.).

AUTHOR CONTRIBUTIONS

M.G. and S.Z. conceived the project. M.G., S.Z., Y-L Z. and X.T. designed the experiments. Yuqi L., M.G., Q.L., Q.Z., S.Y., Yinan L. and Y-J.P. performed cryo-EM analysis. Y-L.Z., Yuqi L., J.J., S.L., M.L., Y.S., Y-Y.Z. and Y.M. performed the functional study. M.G., Y-L.Z., Yuqi L. and Q.L. wrote the manuscript with input from all co-authors.

COMPETING INTERESTS

The authors declare no competing interests.

REFERENCES

1. Giaccari, C., Cecere, F., Argenziano, L., Pagano, A. & Riccio, A. *Trends Genet.* **40**, 880–890 (2024).
2. Weakley, B.S. *Z. Zellforsch.* **85**, 109–123 (1967).
3. Jentoft, I.M.A. et al. *Cell* **186**, 5308–5327.e25 (2023).
4. Chi, P.L. et al. *Nat. Struct. Mol. Biol.* **31**, 115–124 (2024).
5. Xiong, Z.Q. et al. *Nat. Cell Biol.* **24**, 968–980 (2022).
6. Zhang, H.M. et al. *Genome Biol.* **24**, 166 (2023).
7. Li, J.H. et al. *Nat. Struct. Mol. Biol.* **33**, 512–524 (2026).
8. Xu, Y. et al. *Am. J. Hum. Genet.* **99**, 744–752 (2016).
9. Li, L., Baibakov, B. & Dean, J. *Dev. Cell* **15**, 416–425 (2008).
10. Zhang, W.Z. et al. *Cell Rep.* **42**, 113531 (2023).
11. Uemura, S. et al. *Life Sci. Alliance* **6**, e202301904 (2023).
12. Liu, S.X. et al. *Nature* https://doi.org/10.1038/s41586-026-10360-7 (2026).
13. Chi, P.L. et al. *Nature* https://doi.org/10.1038/s41586-026-10442-6 (2026).
14. Kılıç, Z.I. et al. *Nature* https://doi.org/10.1038/s41586-026-10513-8 (2026).
15. Singh, K., Harasimov, K., Niakan, K.K. & Carter, A.P. *BioRxiv* 2026.03.22.713481 (2026).
16. Li, Y.J. et al. *BioRxiv* 2026.03.30.715190 (2026).

ADDITIONAL INFORMATION

Supplementary information The online version contains supplementary material available at https://doi.org/10.15302/vita.2026.04.0030.

Correspondence and requests for materials should be addressed to Xiaomei Tong, Songying Zhang or Miao Gui.